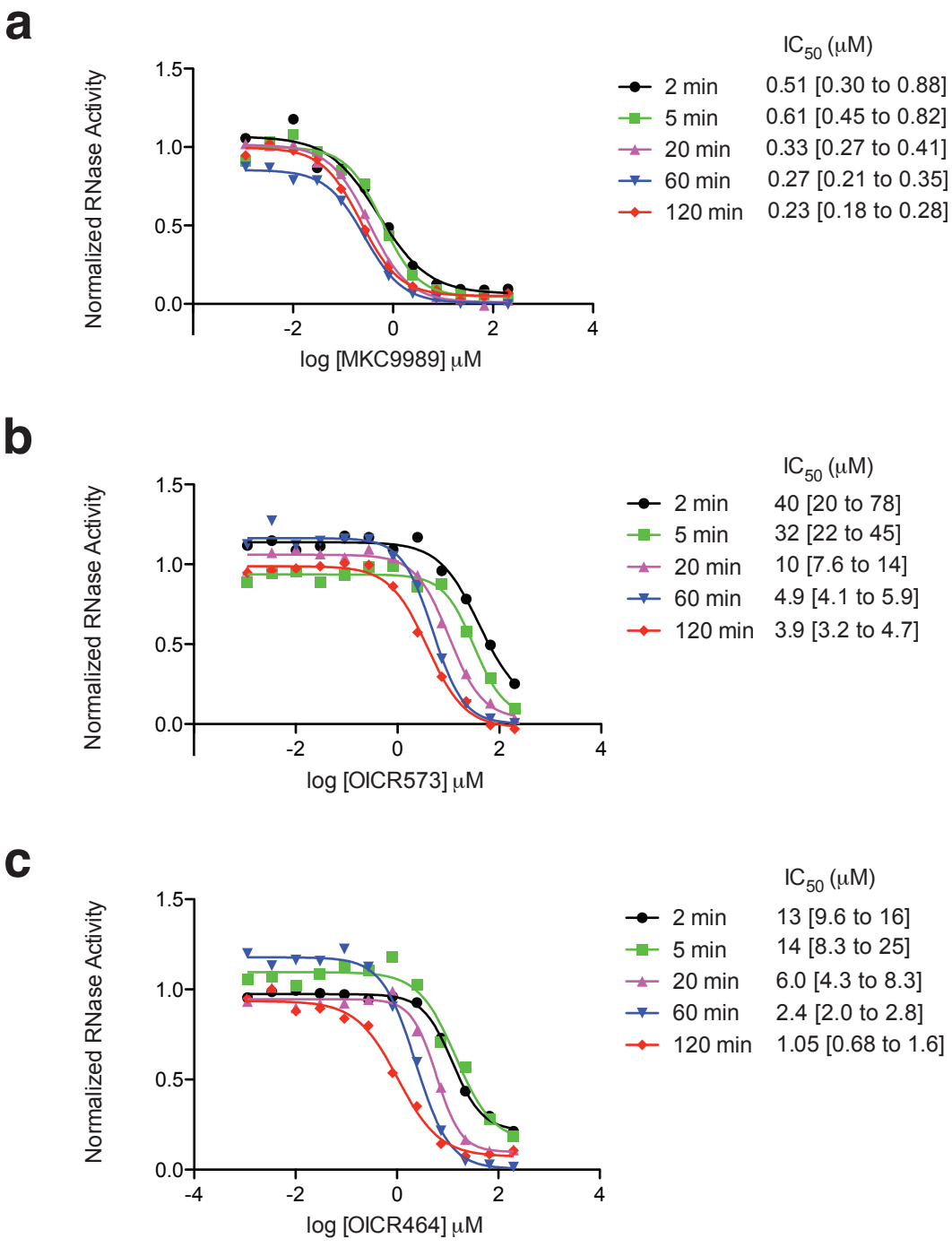

Supplementary Figure 1. Time dependency of inhibition of murine IRE1α RNase activity by MKC9989 **(a)**, OICR573 **(b),** and OICR464 **(c),** using a real time fluorescence readout assay. IC50s and 95% confidence intervals (in brackets) are derived from a single fitted profile through measurments from two experiments.

S2

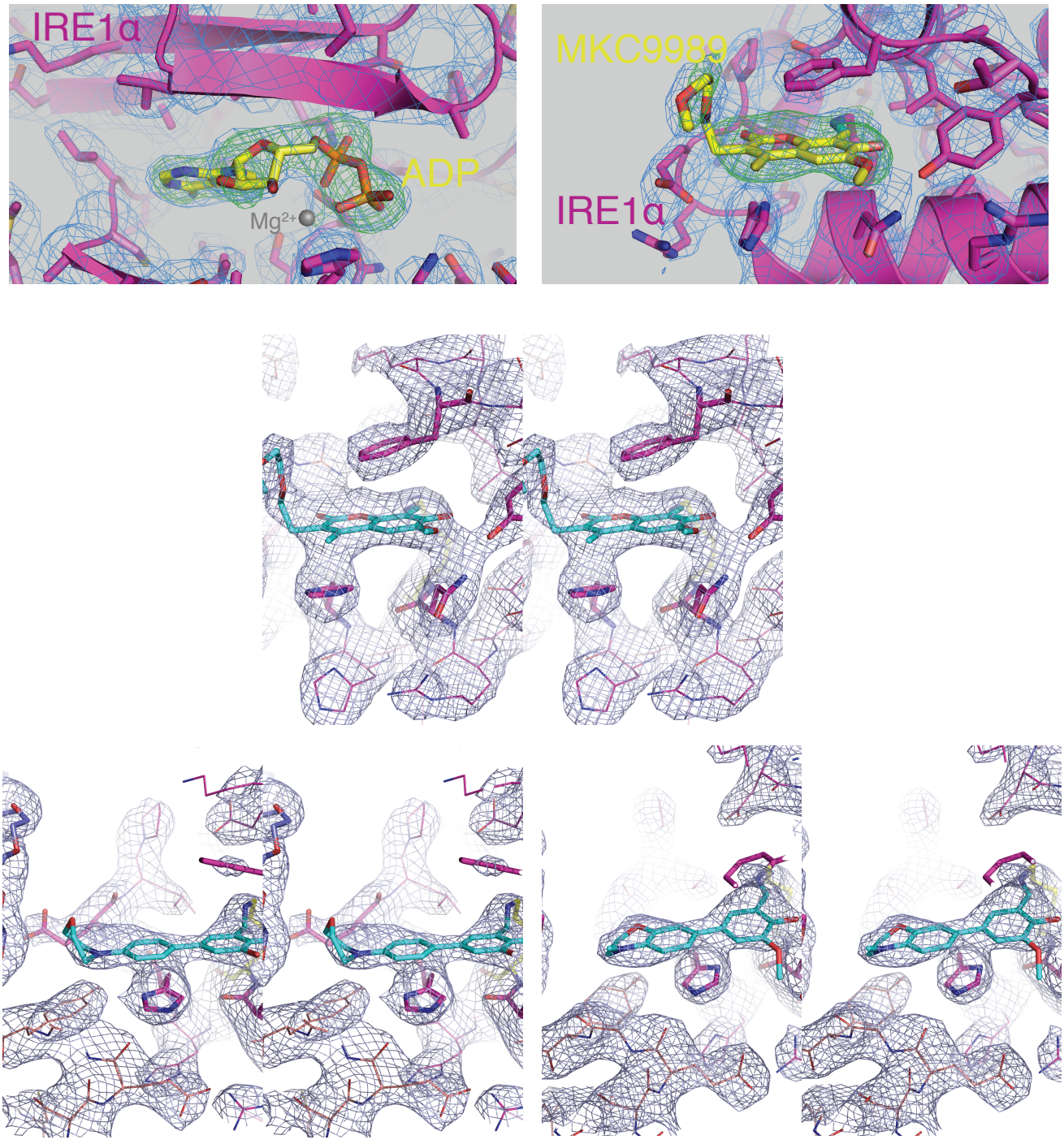

Supplementary Figure 2. (a) Representative electron density maps of ADP engaging the kinase active site (left) and MKC9989 engaging the RNase active site (right) of IRE1α in the IRE1α - MKC9989 co-structure. 2Fo-Fc electron density corresponding to the final refined map contoured at 1.3σ (blue wire mesh). Simulated annealing omit map contoured at 3.0σ for the omitted ligand (green wire mesh). Protein is coloured purple and ligands are coloured with carbon atoms yellow. **(b)** Stereo views of representative 2Fo-Fc electron density maps contoured at 1.5σ (blue wire mesh) centered on the MKC9989 (top), OICR573 (bottom left) and OICR464 (bottom right) binding sites. Protein is coloured purple and ligands are coloured with carbon atoms in blue.

S3

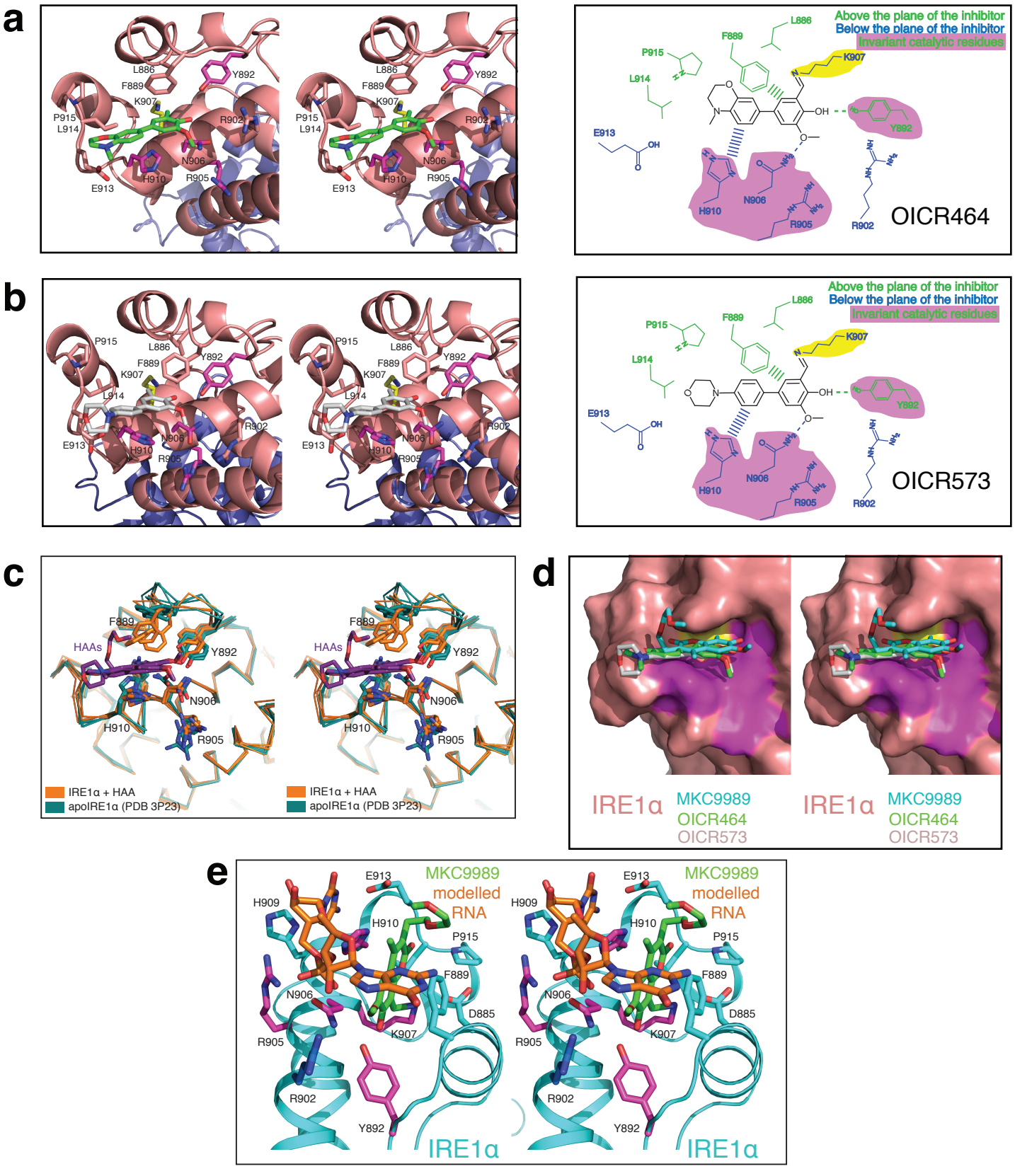

Supplementary Figure 3. Structure of IRE1α bound to OICR464 and OICR573. **(a)** Stereo (left) and schematic (right) representations of OICR464 binding to IRE1α. Colouring as in Figure 3B but with HAA shown in green. **(b)** Stereo (left) and schematic (right) representations of OICR573 binding to IRE1α. **(c)** Stereo view of overlayed binding modes of MKC9989, OICR464 and OICR573 to IRE1α with HAA shown in purple. **(d)** Stereo surface view of overlayed binding modes of MKC9989, OICR464 and OICR573 to IRE1α. **(e)** Structure of IRE1α (blue) bound to MKC9989 (green) and a modeled dinucleotide RNA substrate (orange).

S4

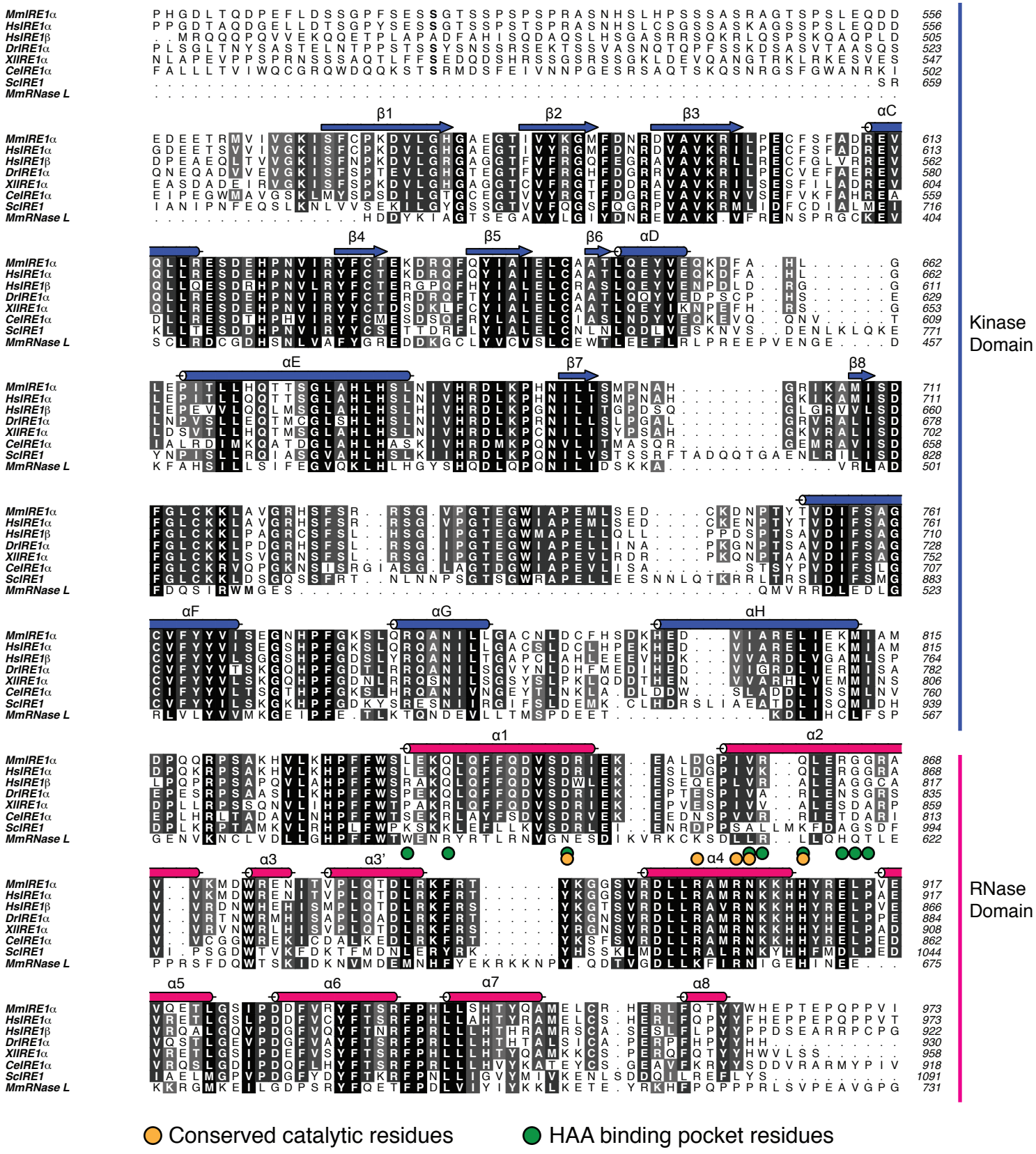

Supplementary Figure 4. Sequence alignment of the cytosolic portion of IRE1 orthologues. The species in the alignment are (top to bottom): Mus musculus, Homo sapiens, Danio rerio, Xenopus laevis, Caenorhabditis elegans, and Saccharomyces cerevisiae. Shown at bottom of the alignment is the sequence of the paralogue Homo sapiens RNase L. The secondary structure of murine IRE1α is highlighted over the sequence.

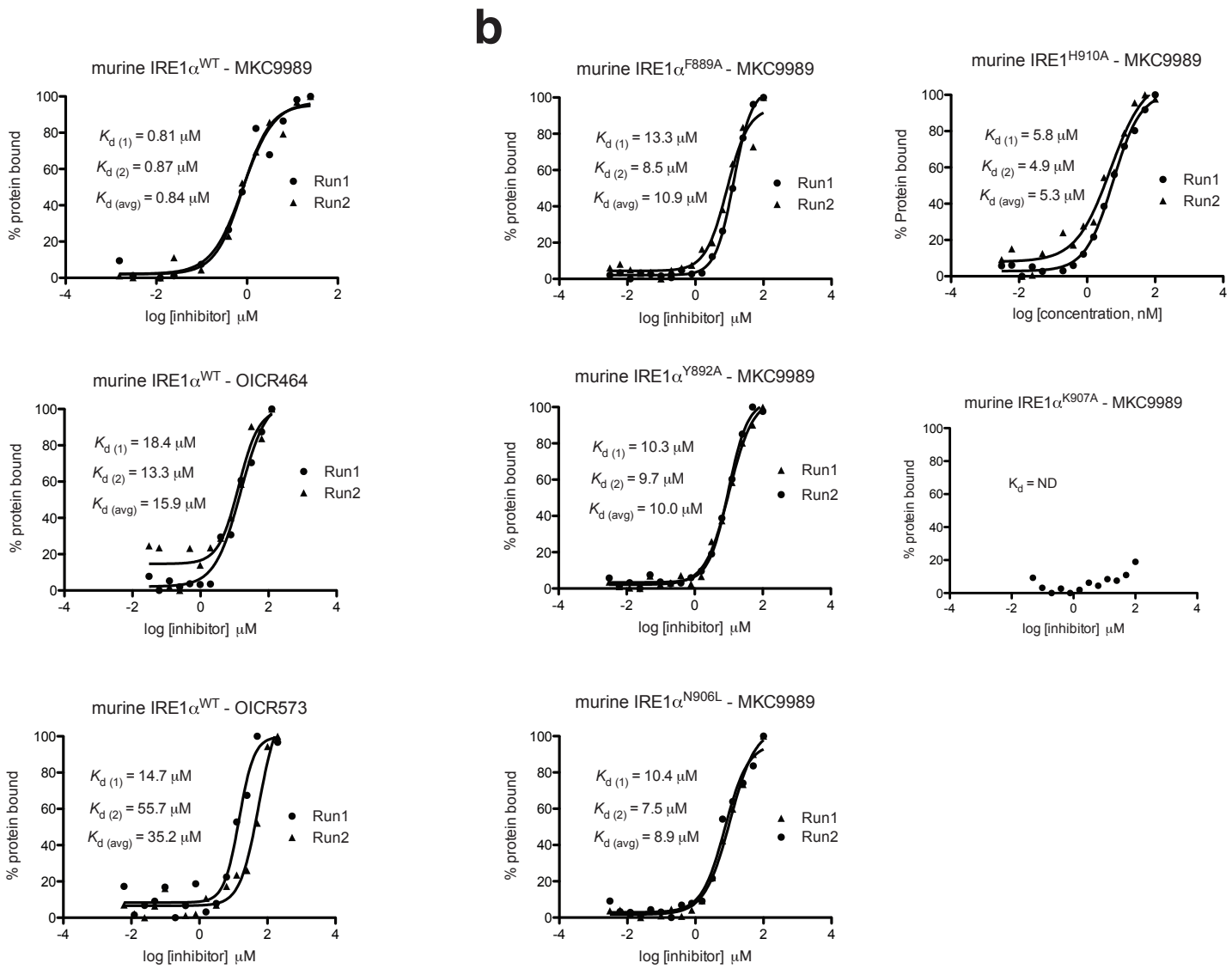

Supplementary Figure 5. Measurement of direct binding of HAA inhibitors to murine IRE1α by micro-scale thermophoresis. **(a)** Binding of murine IRE1α^{WT} to MKC9989, OICR464 and OICR573. **(b)** Binding of MKC9989 to murine IRE1α mutants Phe889Ala, Tyr892Ala, Asn906Leu, His910Ala and Lys907Ala. Shown are the fitted profiles of the two duplicates with the K_d for each as well as the $K_{d\ (average)}$

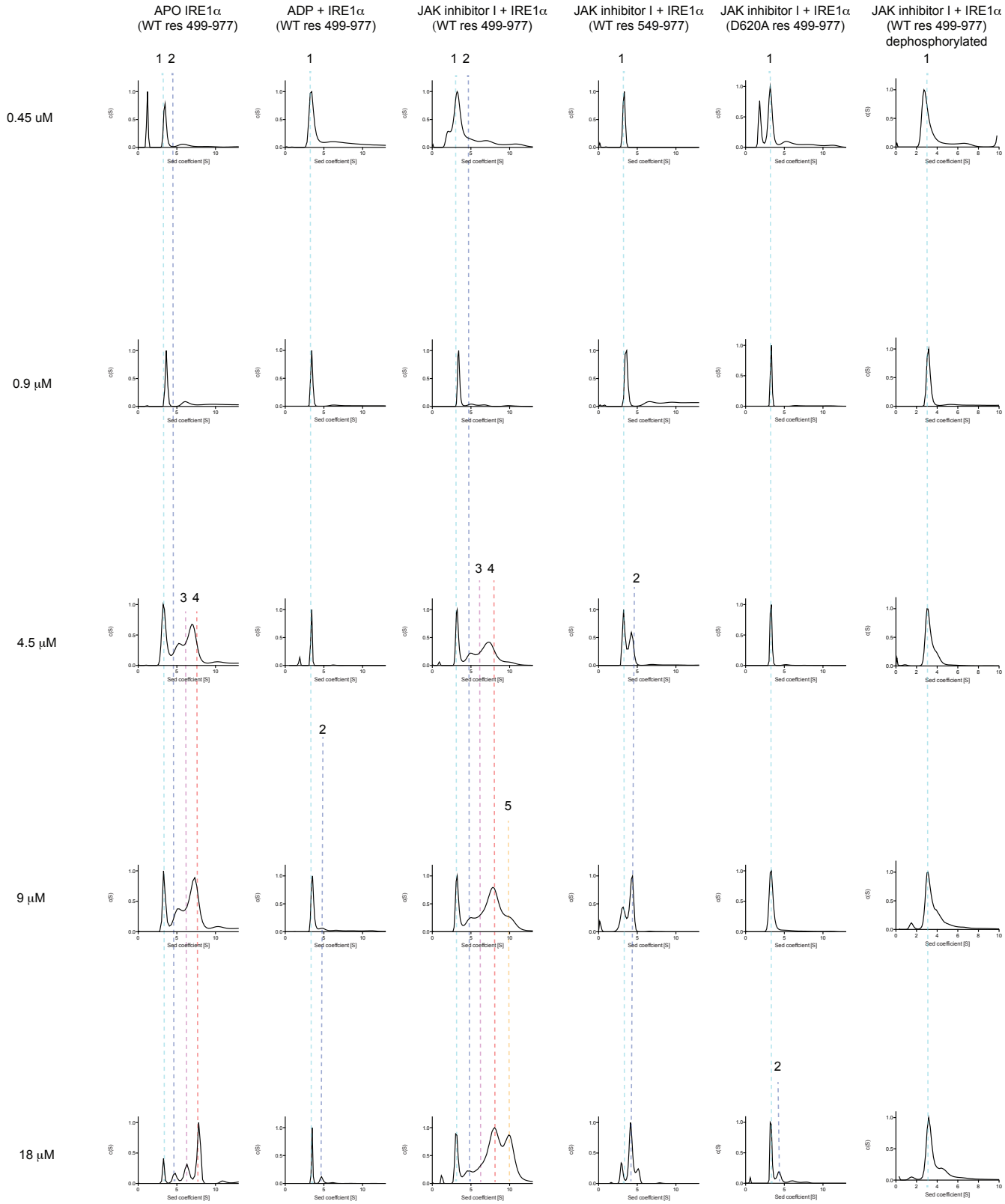

Supplementary Figure 6. Analysis of the oligomerization status of murine IRE1α. Analytical ultracentrifugation analyses were performed on murine IRE1α preparations (labelled at top) at the indicated protein concentrations (labeled at left). Concentrations of ADP and JAK inhibitor I were 500 μM and 30 μM respectively.